

Electronic Supplementary Information (ESI) for ChemComm.

This journal is © The Royal Society of Chemistry 2020

**Nanofabrication of Hollowed-Out Au@AgPt Core-Frames via Selective Carving of Silver and Deposition of Platinum**

Chang Xia,<sup>a</sup> Wei He,<sup>b</sup> Peng Fei Gao,<sup>b</sup> Jia Ru Wang,<sup>a</sup> Zheng Mao Cao,<sup>a</sup> Yuan Fang Li,<sup>\*a</sup> Yi Wang,<sup>\*c</sup> and Cheng Zhi Huang,<sup>\*b</sup>

a. Key Laboratory of Luminescent and Real-Time Analytical Chemistry (Southwest University) Ministry of Education, College of Chemistry and Chemical Engineering, Southwest University, Chongqing 400715 (P. R. China). E-mail:

liyf@swu.edu.cn

b. Key Laboratory of Biomedical Analysis (Southwest University) Chongqing Science and Technology Bureau, College of Pharmaceutical Sciences, Southwest University, Chongqing 400715 (P. R. China). E-mail: chengzhi@swu.edu.cn

c. Chongqing Key Laboratory of Green Synthesis and Applications, College of Chemistry, Chongqing Normal University, Chongqing 401331 (P. R. China). E-mail: ywang@cqnu.edu.cn

## **Experimental section**

### **Materials and Reagents.**

Gold chloride trihydrate ( $\text{HAuCl}_4 \cdot 3\text{H}_2\text{O}$ , >99%) was purchased from Sinopharm Chemical Reagent Co., Ltd (Shanghai, China). Chloroplatinic acid ( $\text{H}_2\text{PtCl}_6$ , 99.95%), cetyltrimethylammonium bromide (CTAB, >99%), cetyltrimethylammonium chloride (CTAC, 97%), sodium borohydride ( $\text{NaBH}_4$ , 99%), silver nitrate ( $\text{AgNO}_3$ , 99.8%), Silver trifluoroacetate ( $\text{CF}_3\text{COOAg}$ , 98%), ascorbic acid (L-AA, >99%) and 4-Mercaptobenzoic acid (4-MBA, 90%) were obtained from Aladdin (Shanghai, China). All reagents were used as received. All solutions were prepared using ultrapure water (18.2 M $\Omega$ ) from a Milli-Q system (Millipore, Bedford, MA, USA).

### **Apparatus.**

Surface properties were performed on an ESCALAB 250 X-ray photoelectron spectrometer (XPS) (Tyoto, Japan). SEM images were collected with a S-4800 field-emission SEM instrument (Hitachi, Japan) at 15 kV. TEM characterization was performed on a FEI Tecnai G2 F20 TEM instrument (FEI, America). Ultraviolet-visible extinction spectra were obtained with a U-3010 spectrometer (Hitachi, Japan). DFM images were real-time captured by a BX73 optical microscope (Olympus, Japan) focused through a U-DCW NA1.2-1.4 high numerical dark-field condenser. The scattered light was collected using a 100 $\times$ oil immersion objective and the images were taken using a DP72 single chip true-color CCD camera (Olympus, Japan). A monochromator was equipped with a SR303i-B spectrograph (Andor, England) and the recording was carried out using a DU970P-BVF CCD spectrometer (Andor,

England) to obtain the scattering spectra. The images were analysed with Image-Pro Plus 6.0 (IPP) software (Media Cybernetics, USA). Raman spectra were recorded on a LabRAM HR800 spectrometer with a laser of 532 nm in the range of 800-1800  $\text{cm}^{-1}$  (Horiba Jobin-Yvon, France). The FDTD simulations were performed on FDTD solutions (Lumerical Solutions, Inc., Vancouver, Canada). All electrochemical measurements were carried out using a CHI 900D instrument (Chenhua, China).

### **Synthesis of ~ 30 nm Au seeds.**

The spherical Au seeds with diameter of ~30 nm were prepared according to the literature method with slight modification.<sup>1</sup> First, 3-nm Au seeds with brownish color were prepared by mixing 5 mL of 0.05 M  $\text{HAuCl}_4$  solution and 5 mL of 0.2 M CTAB solution, and then a 0.6 mL of fresh ice-cold 0.01 M  $\text{NaBH}_4$  was quickly injected into the Au (III) CTAB solution under vigorous stirring for 2 min. The seed solution was aged at room temperature for 3 h before use.

Then, for the growth of CTAC-capped 10 nm Au nanospheres, 0.3 mL of 0.01 M  $\text{HAuCl}_4$  solution, 6 mL of 0.2 M CTAC solution and 3 mL of 0.1 M AA solution were mixed, followed by the addition of 0.3 mL of the 3-nm Au seeds solution. The mixture was left undisturbed for 1 h at 36 °C.

Next, in order to obtain 30 nm Au nanospheres, a growth solution was prepared by dissolving 5 mL of 0.5 mM  $\text{HAuCl}_4$  solution, 5 mL of 0.2 M CTAC solution and 2 mL of 0.1 M AA, followed by the addition of 1 mL of 10 nm nanospheres solution. The mixture was left undisturbed at 36 °C for 1 h. The final products of Au seeds (~ 30 nm) were obtained.

### **Synthesis of Au@Ag CSNs.**

Au@Ag CSNs were prepared using a seed-mediated growth process developed by Xia and co-workers with slight modification.<sup>2</sup> Firstly, spherical Au seeds with diameter of ~30 nm were prepared according to the literature method with slight modification.<sup>3</sup> The details for the synthesis were shown in the Supporting Information. Then, the Au@Ag CSNs were synthesized by depositing Ag onto ~30 nm Au seeds. In brief, 3 mL of the prepared ~30 nm Au seeds, 7 mL of 0.2 M CTAC solution and 3 mL of 0.1 M AA solution were mixed at 60 °C, followed by injecting 0.4 mL of 0.01 M AgNO<sub>3</sub> solution at a rate of 0.06 mL min<sup>-1</sup> using a syringe pump, and was further kept undisturbed at 60 °C for 4 h. The obtained Au@Ag CSNs were centrifugally washed with water twice.

### **Synthesis of Ag-Pt NCs.**

Ag NCs were prepared using a seed-mediated growth process developed by Huang et al.<sup>4</sup> Firstly, the Ag seeds were prepared by mixing 25 µL of 0.1 M AgNO<sub>3</sub> solution and 10 mL of 0.5 mM CTAC solution, and then a 0.45 mL of fresh ice-cold 0.02 M NaBH<sub>4</sub> was quickly added with stirring. The resulting solution immediately turned yellow, indicating the formation of silver nanoparticles. The seed solution was aged at room temperature for 40 min before use. Then, 8.60 mL of deionized water containing 0.04 g CTAC, 300 µL of the seed solution and 100 µL of 0.1M CF<sub>3</sub>COOAg solution were mixed and kept in a water bath at 60 °C for 20 min. Next, 1 mL of 0.1 M AA solution was added and the solution was stirred for 1.5 h at 60 °C. The obtained Ag NCs were centrifugally washed with water twice. Last, 0.5 mL of Ag NCs suspension and 25 µL of 1 mM H<sub>2</sub>PtCl<sub>6</sub> aqueous solution were mixed. The

reaction mixture was quenched through centrifugation twice after 60 min.

### **Ex situ Monitoring of the Plasmonic Evolution.**

In a standard protocol, 0.3 mL of Au@Ag CSNs suspension and 7.5  $\mu\text{L}$  of  $\text{H}_2\text{PtCl}_6$  aqueous solution (1 mM) were mixed. Then, the reaction mixture was quenched through centrifugation twice at different reaction time (10min, 30min, 60min), followed by an examination of the reaction products. To measure the scattering signals under a surrounding aqueous medium at a single particle level, 100  $\mu\text{L}$  of products were deposited on an indium-tin-oxide glass and left for 30 min and then flushed with water to remove the non-adsorbed products. A drop of water was filled inside the frame which consists of the slide glass and a thin cover. It is worth mentioning that, in order to achieve colocation of the same nanoparticles under DFM and SEM, a label was previously marked on the glass slide. SEM images of the same collection of products were taken with low and high magnification.

### **In situ Monitoring of the Plasmonic Evolution.**

First, the Au@Ag CSNs were immobilized on the glass slide surface with a suitable density. To real-time monitor the evolution of GR reaction, a homemade microfluidic cell was utilized. An area containing blue-green scattering light Au@Ag CSNs was selected for real-time observation. Then, 200  $\mu\text{L}$  of  $\text{H}_2\text{PtCl}_6$  aqueous solution (20  $\mu\text{M}$ ) was added into the flow cell. Next, consecutive DFM images in the same area were recorded with BX73 optical microscope at a rate of 1 frame per minute.

### **In Situ SERS Measurements in the Reaction Solution.**

In a typical study, 10  $\mu\text{L}$  of 0.01 M 4-MBA ethanol solution were added to 1 mL of

Au@Ag CSNs aqueous solution. The mixed solution was incubated at room temperature for 2h. Then, we collected the 4-MBA-functionalized Au@Ag CSNs by centrifugation and washed with water prior to characterization. We took 0.3 mL of the 4-MBA-functionalized Au@Ag CSNs and mixed it with 7.5  $\mu$ L of H<sub>2</sub>PtCl<sub>6</sub> aqueous solution (1 mM) to start the reaction at room temperature. We sampled an aliquot of 20  $\mu$ L from the reaction solution every several minutes and collect the SERS spectrum for monitoring the progress of the reaction.

### **FDTD Simulations.**

A wavelength range from 450 to 600 nm was radiated into a box containing a model of a nanostructure (dielectric functions of Au, Ag and Pt were taken from the experimental data conducted by palik). The surrounding medium inside the box was divided into the meshes of 0.5 nm, and its refractive index was set to be 1.33 and 2.06 for water and AgCl, respectively. The diameters in the model were used for the calculations based on the TEM image.

### **HER Electrochemical Characterization.**

A working electrode was made by drop casting 100  $\mu$ L of the catalyst to cover an ITO slide (1 cm<sup>2</sup>). A graphite rod was used as the counter electrode. An Ag/AgCl electrode was used as the reference for all the electrochemical tests, and the potential was calibrated to the reversible hydrogen electrode (RHE) for the tests of HER (the potential of the Ag/AgCl is 0.238 V versus RHE).

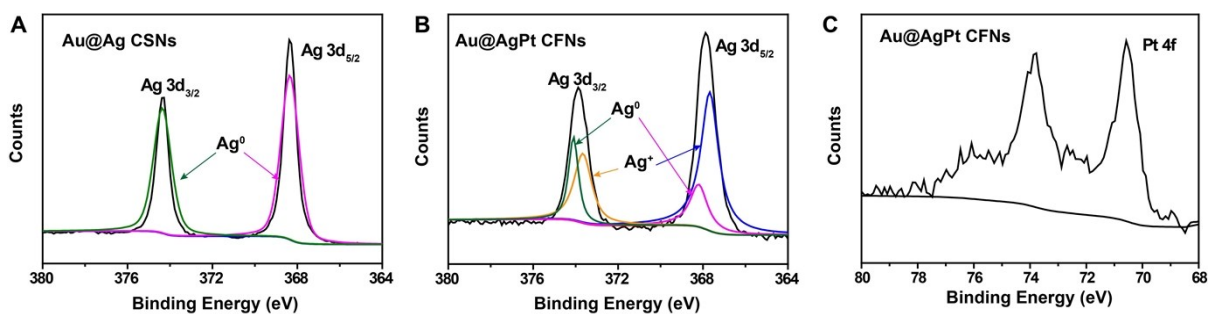


**Figure S1.** (A and B) High-resolution Ag3d spectra of Au@Ag CSNs and Au@AgPt CFNs, respectively. (C) High-resolution Pt4f spectrum of Au@AgPt CFNs.

As shown in Figure S1, the surface properties of the Au@Ag CSNs and Au@AgPt CFNs were determined by X-ray photoelectron spectroscopy (XPS). In Figure S1A, the high-resolution spectrum of Au@Ag CSNs shows that Ag 3d<sub>5/2</sub> and 3d<sub>3/2</sub> peaks were located at 368.3 and 374.1 eV, characteristic of Ag in its metallic state. For Au@AgPt CFNs, both Ag 3d<sub>5/2</sub> and 3d<sub>3/2</sub> peaks (Figure S1B) can be divided into two separate peaks. Among them, the peaks at 367.7 and 373.7 eV are attributed to Ag<sup>+</sup> in AgCl, and those at 368.2 and 374.1 eV are assigned to Ag<sup>0</sup> species.<sup>5</sup> These results indicated that Ag may exist in the forms of both Ag/Pt alloy and AgCl. For Pt 4f<sub>7/2</sub>, typical binding energies are 73-74.2 eV for K<sub>2</sub>PtCl<sub>4</sub>, 71.1 eV for Pt, and 70.9-70.2 eV for Pt/Ag alloys, respectively.<sup>5</sup> For our sample, the Pt 4f<sub>7/2</sub> peak from the high-resolution spectrum is located at 70.7 eV (Figure S1C), meaning that Pt mainly exists in alloy form. This observation suggests that indicate the presence of Pt/Ag alloy and AgCl in Au@Ag CSNs.

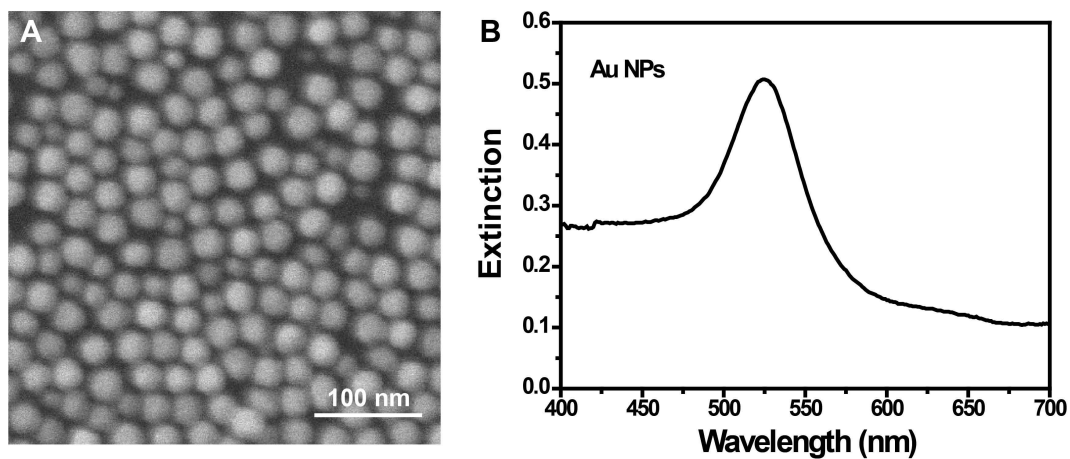


**Figure S2.** (A) Scanning electron microscopy (SEM) image and (B) Localized surface plasmon resonance (LSPR) extinction spectrum of Au nanoparticles. The LSPR peak is located at 524 nm.

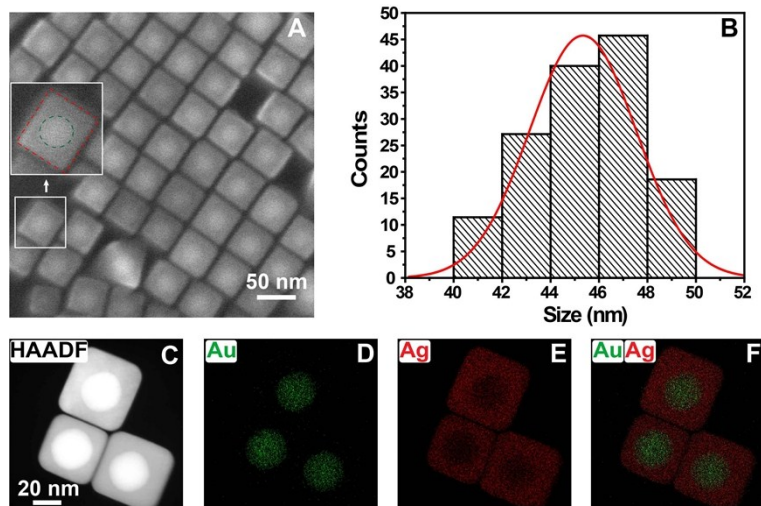


**Figure S3.** Morphological and elemental characterizations of the Au@Ag CSNs: (A) SEM image; (B) Size distribution histogram; (C) HAADF-STEM image and (D-F) the corresponding STEM-EDS chemical maps. (D) and (E) show the EDS signal of Au and Ag, respectively, while (F) displays the signals of Au and Ag simultaneously.

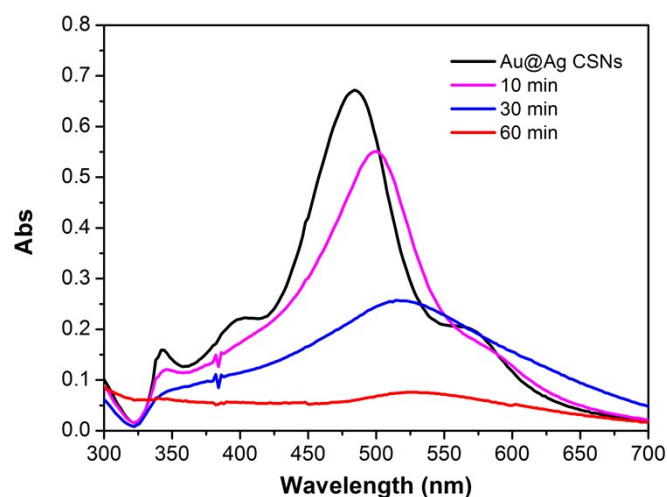


**Figure S4.** Time-dependent extinction spectra evolution of Au@Ag CSNs solutions.

Following the change in morphology and composition of the nanocrystals (Fig. 1), the LSPR properties of these nanostructures at different reaction stages which are greatly related to the structure and composition of the nanocrystals and their surface electron states also, were accordingly changed.<sup>6</sup> The Au@Ag CSNs solution exhibited a characteristic strong in-plane dipole absorption band centered at 484 nm and three weak LSPR bands located at 347, 390, and 570 nm, respectively (Fig. S4). These bands characterized at 347 and 390 nm indicated that the Au@Ag CSNs with sharp corners had been formed, while the shoulder peak at 570 nm could be due to the small amount of right pyramidal nanocrystals (Fig. S3A).<sup>2</sup> The main LSPR band at 484 nm displayed a constant red-shift and decrease in absorbance as the GR reaction proceeded in the presence of  $\text{PtCl}_6^{2-}$  precursor (Fig. S4). The other three bands even disappeared with the end of the reaction. These results suggested that the optical properties of the nanostructure are tunable through the visible colour change of solution. Combining the aforementioned evolution of morphologies (Fig. 1), we supposed that the gradual red-shift of the LSPR bands was attributed to the emergence of cavities on the nanocrystals and the degree of hollow structures increases along with reaction.<sup>7</sup> The decrease of these LSPR bands was on account of the dissolution of Ag atoms from the  $\{100\}$  facets and the deposition of Pt atoms on the active edges.

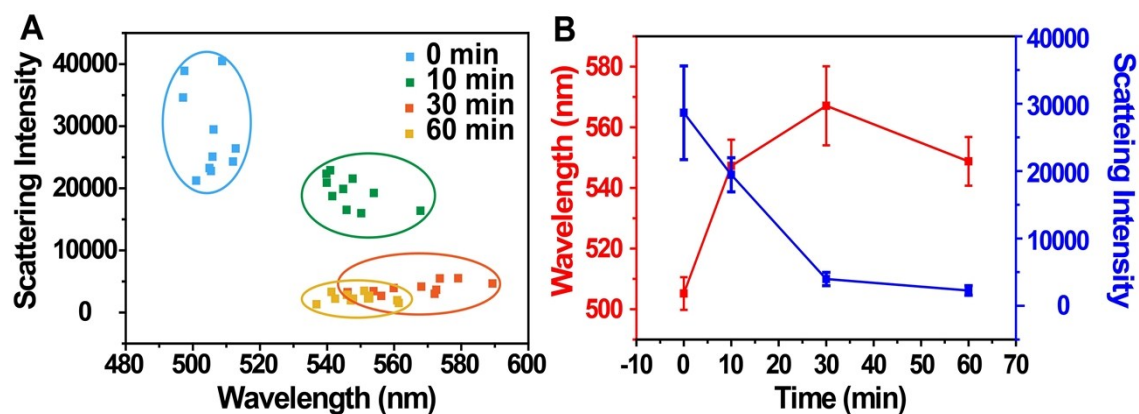


**Figure S5.** LSPR scattering spectral study of single nanoparticles in different stages of the GR reaction. (A) Distributions of LSPR scattering bands of randomly selected 10 individual particles in different stages of the GR reaction. Blue, green, orange, and yellow data represent the peak wavelengths and intensities at 0, 10, 30 and 60 min, respectively. (B) Trajectories of the maximum LSPR scattering wavelength (red line) and intensity (blue line) of individual particles during the GR reaction. Error bars are calculated from 10 particles ( $n=10$ ).

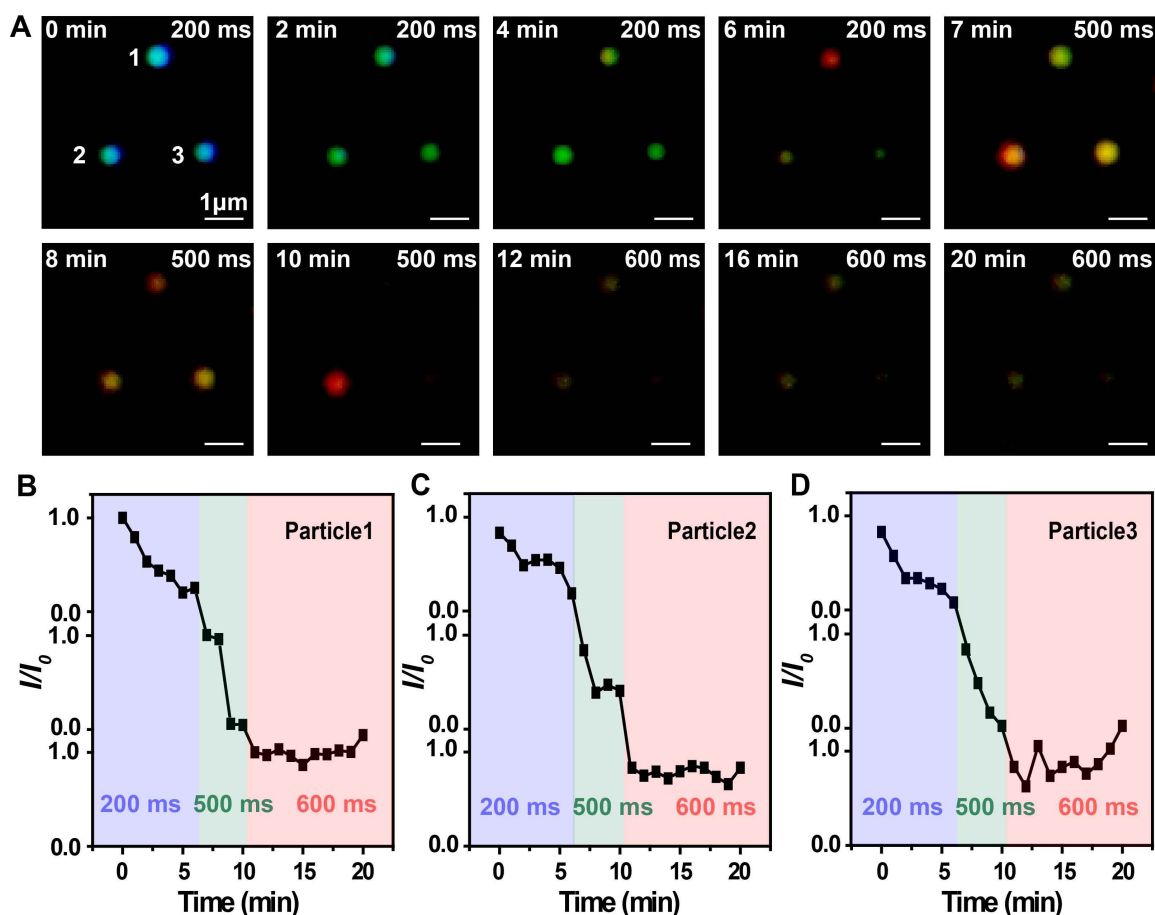


**Figure S6.** DFM scattering signals of individual Au@Ag CSNs during the GR reaction in the presence of  $\text{PtCl}_6^{2-}$  precursor. (A) DFM images captured at different time points. Time-dependent intensity analysis of (B) particle 1, (C) particle 2 and (D) particle 3 that is shown in (A), respectively. 200, 500 and 600 ms in (A) to (D) represent different exposure time of CCD.

Since the LSPR scattering intensity of the particles gradually decreased along with the GR reaction, a longer exposure time had to be taken from the initial 200 ms to the final 600 ms so that the particles were able to be observed owing to the decreasing scattering signals. In order to obtain the quantitative information of a specific particle in the GR process, the LSPR scattering light intensities, however, significantly decreased to  $\sim 10\%$  of its original intensity within 6 min (Fig. S6B), demonstrating that the LSPR scattering intensity of the nanoparticles decreased sharply at the initial reaction period. The LSPR scattering light intensities continuously decreased from 7 to 11 min and maintained unobvious changes in the

final stage (12–20 min). Also, like the result above-mentioned of the ex situ experiment, the dissolved of Ag atoms and morphological change of the Au@Ag CSNs lead to decrease of the LSPR scattering light intensities, while the deposition of Pt atoms had a relatively small contribution.

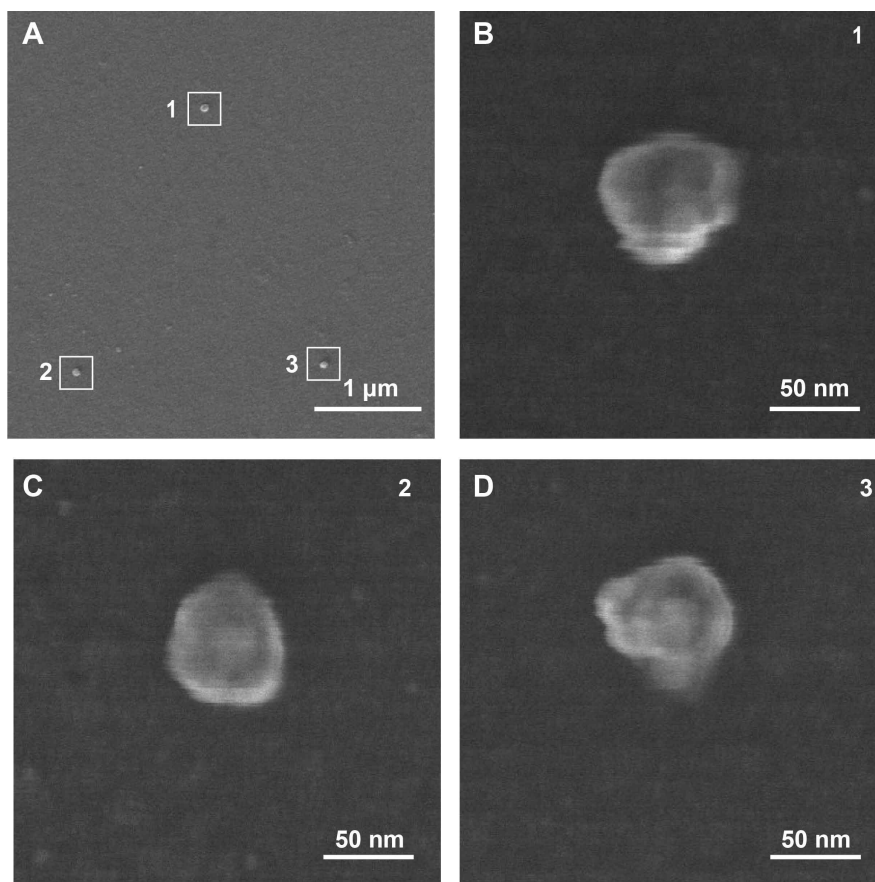


**Figure S7.** Colocation SEM images of Au@AgPt CFNs corresponding particle 1-3 after the GR reaction in Figure S5. (A) SEM image in the same collection of Au@AgPt CFNs. (B-D) SEM images of numbered Au@AgPt CFNs in (A) with high magnification, respectively.

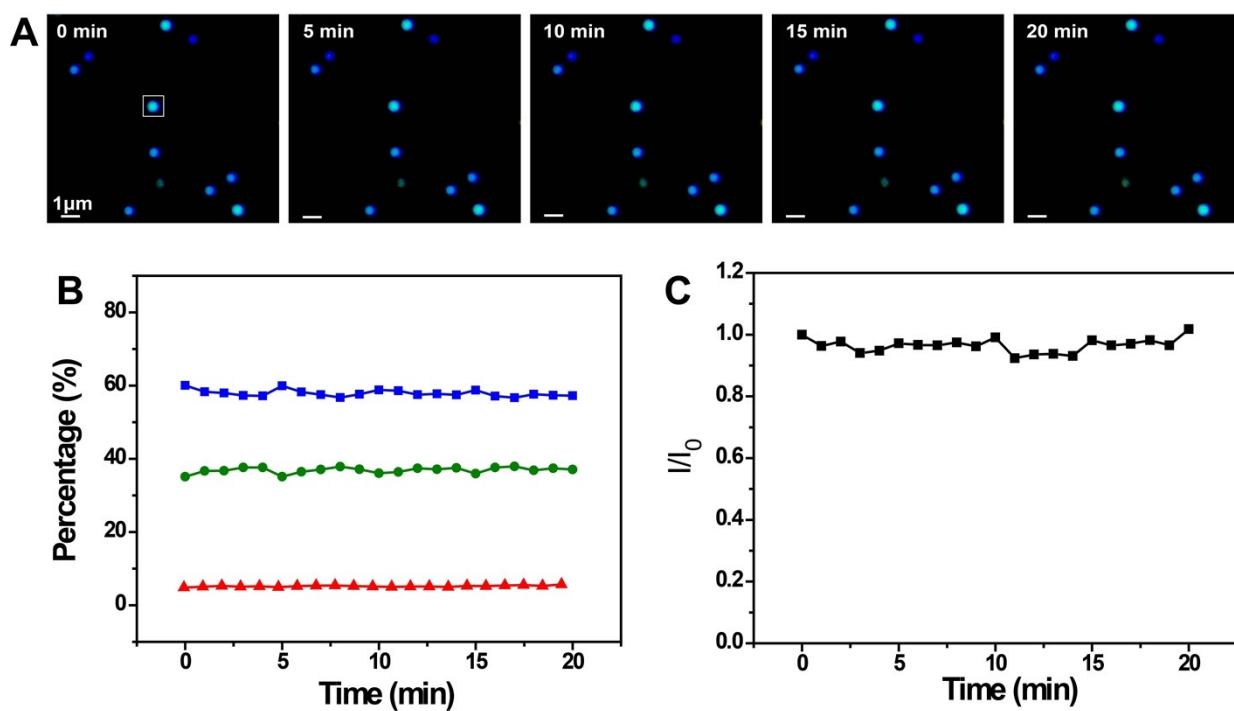


**Figure S8.** Dark-field light scattering signals of an individual Au@Ag CSN with ultrapure water. (A) Time-dependent images captured at different time points. (B) Time-dependent RGB and (C) intensity analysis of corresponding particle 1 in (A). The RGB and scattering intensity of the chosen Au@Ag CSN remained the same before and after the reaction, accompanied by a small mechanical error.

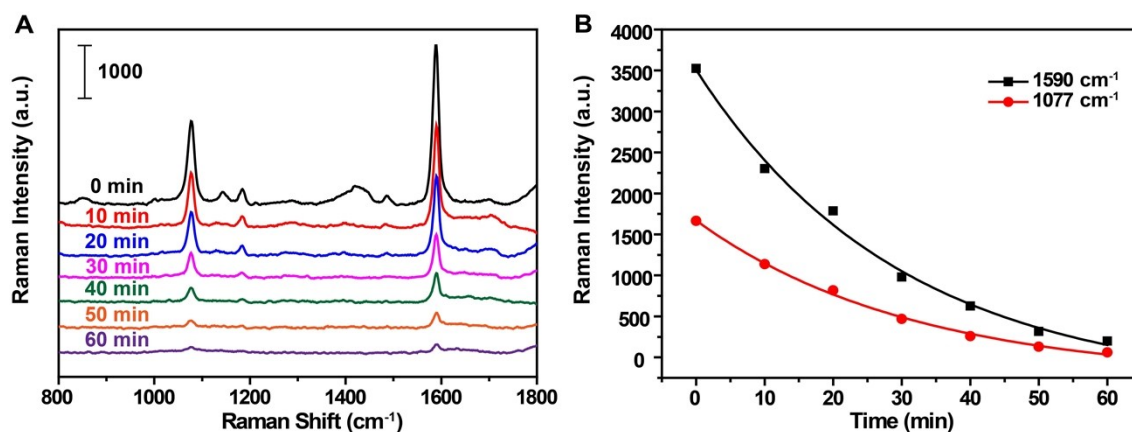


**Figure S9.** Time-dependent SERS spectral study of 4-MBA recorded from an aqueous mixture of Au@Ag CSNs and  $\text{PtCl}_6^{2-}$  precursor up to 60 min. (A) Time-dependent SERS spectra. (B) Time-dependent intensities of the bands at 1077 and 1590  $\text{cm}^{-1}$  in the SERS spectra of (A), respectively.

The intense and characteristic SERS of 4-MBA located at 1077  $\text{cm}^{-1}$  and 1590  $\text{cm}^{-1}$  (Fig. S9) are assigned to the in-plane ring breathing mode coupled with  $\nu(\text{C-S})$  and the aromatic  $\nu(\text{CC})$  mode, respectively.<sup>8</sup> The decrease of SERS intensity of the two peaks were observed (Fig. S9B), and the rate of decrease, namely, the slope of curves became flat as the reaction progressed to 60 min. Combined with the morphological evolution mentioned above, we supposed that dramatic change of SERS intensity was due to the dissolution of a mess of Ag atoms from the  $\{100\}$  facets of Au@Ag CSNs into the solution. Moreover, Pt atoms would be selectively deposited on the edges of nanocubes (i.e., hot spots for SERS) and ultimately activated the damper effect of Pt on the SERS properties.<sup>9</sup>

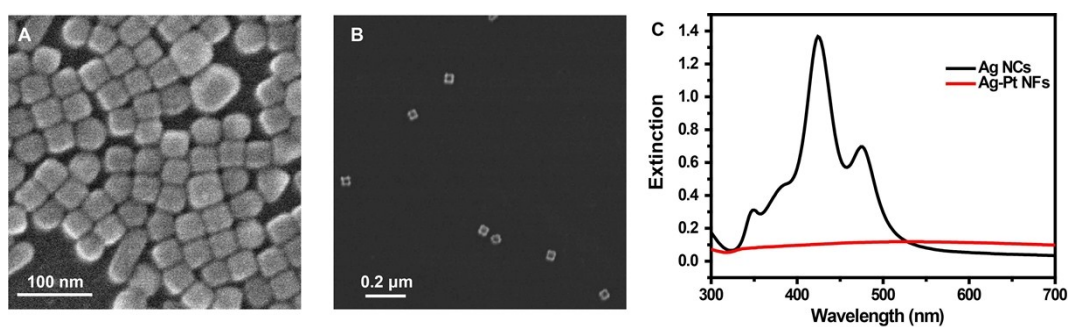


**Figure S10.** Scanning electron microscopy image of Ag NCs (A) and Ag-Pt NFs (B). (C) LSPR extinction spectra of Ag NCs and Ag-Pt NFs.

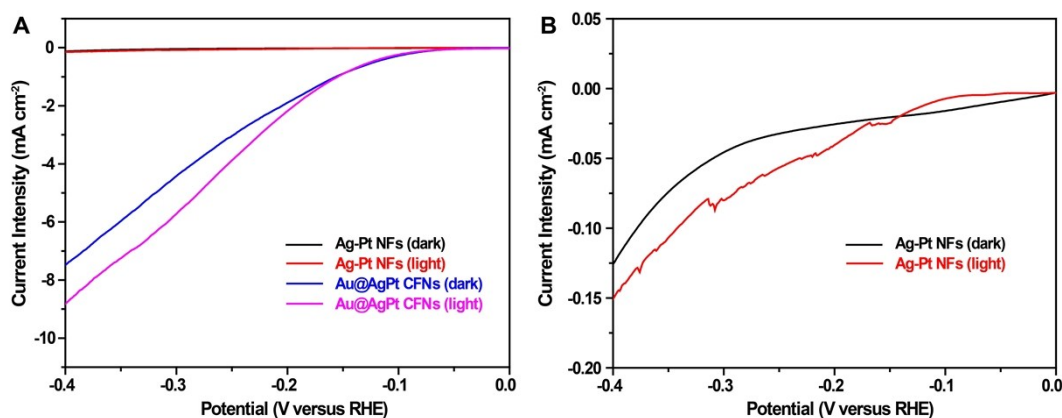


**Figure S11.** (A) LSV curves of different nanomaterials in dark and visible light in a 0.5 M H<sub>2</sub>SO<sub>4</sub> solution (pH = 0.76) using a typical three-electrode configuration at 30 °C. (B) The enlarged LSV curves of Ag-Pt NFs in dark and visible light.

As a proof of concept, the high performances of the Au@AgPt CFNs were further identified through a plasmon-enhanced electrocatalytic hydrogen evolution reaction (HER) as compared to Ag-Pt nanoframes<sup>10</sup> (Ag-Pt NFs) (Fig. S10). The Au@AgPt CFNs show significantly higher electrocatalytic activity than the Ag-Pt NFs toward the HER either in the dark or under visible light irradiation (Fig. S11). Most importantly, the HER performance of the Au@AgPt CFNs was obviously improved under visible light irradiation as compared to that in the dark. This enhancement effect on the HER was contributed by the photoelectrocatalytic effect from the hot electrons by LSPR excitation.<sup>11</sup> From the enlarged LSV curves of Ag-Pt NFs in dark and visible light (Fig. S11), Ag-Pt NFs also show higher electrocatalytic activity under visible light irradiation. This is because Ag nanoparticles have LSPR properties, hot electrons also could be excited under light irradiation to improve the HER activity. Therefore, such Au@AgPt CFNs with good LSPR performance were able to generate hot electrons under light irradiation to enhance the photocatalytic activity and accelerate the electrochemical processes, which would be promising in the applications of solar-energy harvesting and conversions.

## REFERENCES

- (1) Y. Tian, Z. Shuai, J. Shen, L. Zhang, S. Chen, C. Song, B. Zhao, Q. Fan, L. Wang, *Small* 2018, **14**, 1800669.
- (2) Y. Ma, W. Li, E. C. Cho, Z. Li, T. Yu, J. Zeng, Z. Xie and Y. Xia, *ACS Nano*, 2010, **4**, 6725.
- (3) H. Ting, D. Ying, X. Pengyu, X. Shaobo, S. Yangbin, N. Weihai, Y. Baohua and Z. Xiaochun, *Small*, 2016, **12**, 5049.
- (4) W. Zhang, J. Yang, X. Lu, *ACS nano*, **2012**, *6*, 7397.
- (5) Z.-W. Lin, Y.-C. Tsao, M.-Y. Yang and M. H. Huang, *Chem. Eur. J.*, 2016, **22**, 2326.
- (6) L. Russo, F. Merkoçi, J. Patarroyo, J. Piella, A. Merkoçi, N. G. Bastús and V. Puntès, *Chem. Mater.*, 2018, **30**, 5098.
- (7) J. Chen, B. Wiley, J. McLellan, Y. Xiong, Z.-Y. Li and Y. Xia, *Nano Lett.*, 2005, **5**, 2058.
- (8) Y. Wang, W. Ji, H. Sui, Y. Kitahama, W. Ruan, Y. Ozaki and B. Zhao, *J. Phys. Chem. C*, 2014, **118**, 10191.
- (9) Y. Zhang, J. Liu, J. Ahn, T.-H. Xiao, Z.-Y. Li and D. Qin, *ACS Nano*, 2017, **11**, 5080.
- (10) X. Yang, L. T. Roling, M. Vara, A. O. Elnabawy, M. Zhao, Z. D. Hood, S. Bao, M. Mavrikakis and Y. Xia, *Nano Lett.*, 2016, **16**, 6644.
- (11) Y. Shi, J. Wang, C. Wang, T.-T. Zhai, W.-J. Bao, J.-J. Xu, X.-H. Xia and H.-Y. Chen, *J. Am. Chem. Soc.*, 2015, **137**, 7365.